Reactivity of the Human Thioltransferase (Glutaredoxin) C7S, C25S, C78S, C82S Mutant and NMR Solution Structure of Its Glutathionyl Mixed Disulfide Intermediate Reflect Catalytic Specificity[†,‡]

Yanwu Yang,[§,∥] Shu-chuan Jao,[§,⊥,#] Sambasivarao Nanduri,[∥] David W. Starke,[⊥] John J. Mieyal,*[,⊥,#] and Jun Qin*[,∥,⊥]

Structural Biology Program and Department of Molecular Cardiology, Lerner Research Institute, The Cleveland Clinic Foundation, 9500 Euclid Avenue, Cleveland, Ohio 44195, and Department of Pharmacology, School of Medicine, and Department of Chemistry, Case Western Reserve University, Cleveland, Ohio 44106-4965

Received March 20, 1998; Revised Manuscript Received September 24, 1998

ABSTRACT: Human thioltransferase (TTase) is a 12 kDa thiol−disulfide oxidoreductase that appears to play a critical role in maintaining the redox environment of the cell. TTase acts as a potent and specific reducing agent for protein-S-S-glutathione mixed disulfides (protein-SSG) likely formed during oxidative stress or as redox intermediates in signal transduction pathways. Accordingly, the catalytic cycle of thioltransferase itself involves a covalent glutathionyl enzyme disulfide intermediate (TTase-C22-SSG). To understand the molecular basis of TTase specificity for the glutathione moiety, we engineered a quadruple Cys to Ser mutant of human TTase (C7S, C25S, C78S, and C82S) which retains only the active site cysteine residue (C22), and we solved its high-resolution NMR solution structure in the mixed disulfide intermediate with glutathione (QM-TTase-SSG). This mutant which cannot form a C22-S-S-C25 intramolecular disulfide displays the same catalytic efficiency (V_{max}/K_M) and specificity for glutathionyl mixed disulfide substrates as wild-type TTase, indicating that the Cys-25-SH moiety is not required for catalysis or glutathionyl specificity. The structure of human thioltransferase is characterized by a thioredoxin-like fold which comprises a four-stranded central β-sheet flanked on each side by α-helices. The disulfide-adducted glutathione in the TTase-SSG complex has an extended conformation and is localized in a cleft near the protein surface encompassing the residues from helices-α2,α3, the active site loop, and the loop connecting helix-α3 and strand-β3. Numerous van der Waals and electrostatic interactions between the protein and the glutathione moiety are identified as contributing to stabilization of the complex and confering the substrate specificity. Comparison of the human thioltransferase with other thiol−disulfide oxidoreductases reveals structural and functional differences.

Cells maintain a reduced intracellular state while facing a highly oxidizing extracellular enviroment. Within cells, modulation of the thiol−disulfide status of critical cysteine residues on proteins is being recognized as an important mechanism of oxidative signal transduction and an important consequence of oxidative stress associated with aging and various disease states, including cardiovascular and neurodegenerative diseases and AIDS. Thiol−disulfide oxidoreductases (TDOR)[1] are a group of enzymes that play a key role in maintaining the cellular redox status of sulfhydryl groups through thiol−disulfide exchange reactions (see reviews *1*−*5*). The TDOR family includes thioltransferase [TTase, also known as glutaredoxin (GRx)], thioredoxin (TRx), and protein disulfide isomerase (PDI), together with their respective reducing systems, namely, glutathione (GSH)

[†] Supported in part by grants from the American Cancer Society and the Ohio Board of Regents to J.Q.; and from the American Heart Association, the American Cancer Society (Cuyahoga County Unit of Ohio), the Ohio Board of Regents (Pharmacological Sciences Consortium), and the Veteran's Administration Merit Review to J.J.M. Part of this work contributes to fulfillment of requirements for the Ph.D. degree for S.J.

[‡] The structure coordinates have been deposited in the Brookhaven Protein Data Bank (Accession No. BNL-25360).

* To whom correspondence should be addressed. Jun Qin, Ph.D.: Department of Molecular Cardiology, FF10, Lerner Research Institute, The Cleveland Clinic Foundation, 9500 Euclid Ave., Cleveland, OH 44195; (216)-444-5392 (Phone), (216)-444-9263 (Fax), qinj@cesmtp.ccf.org (E-mail).

* To whom correspondence should be addressed. John J. Mieyal, Ph.D.: Department of Pharmacology, School of Medicine, Case Western Reserve University, 2109 Adelbert Rd., Cleveland, OH 44106; (216)-368-3383(Phone), (216)-368-3395 (Fax), jjm5@po.cwru.edu (E-mail).

[§] Denotes equal contribution.

[∥] Lerner Research Institute, The Cleveland Clinic Foundation.

[⊥] Department of Pharmacology, Case Western Reserve University.

[#] Department of Chemistry, Case Western Reserve University.

[1] Abbreviations: CSSG, cysteinyl-glutathione disulfide; GSH, glutathione; GRx, glutaredoxin; GRx-SSG, *E. coli* GRx in a mixed disulfide intermediate with GSH at Cys-11; HOHAHA, homonuclear Hartman−Hahn; HSQC, heteronuclear single quantum coherence; IPTG, isopropyl-β-D-galactopyranoside; NMR, nuclear magnetic resonance; NOE, nuclear Overhauser effect; NOESY, NOE spectroscopy; PDI, protein disulfide isomerase; PCR, polymerase chain reaction; QM-TTase, quadruple mutant of human thioltransferase (C7S, C25S, C78S, and C82S); QM-TTase-SSG, quadruple mutant of human thioltransferase (C7S, C25S, C78S, and C82S) in the mixed disulfide intermediate with glutathione at Cys-22; TDOR, thiol−disulfide oxidoreductases; ppm, parts per million; TM-TTase, triple mutant of human thioltransferase (C7S, C78S, and C82S); TRx, thioredoxin; TTase, human thioltransferase; TTase-SSG, TTase in the mixed disulfide intermediate complex with glutathione at Cys-22; WT-TTase, wild-type human thioltransferase.

10.1021/bi9806504 CCC: $15.00
Published on Web 11/13/1998

and glutathione disulfide (GSSG) reductase for TTase and PDI, and thioredoxin reductase, all utilizing NADPH as the cofactor. While displaying structural similarities such as the so-called thioredoxin fold and a Cys-X-X-Cys motif at their respective active sites, the three TDOR enzymes exhibit certain remarkable catalytic differences. For example, TRx catalyzes the reduction of intramolecular and mixed disulfides, and its catalytic cycle involves an interchange between dithiol and intramolecular disulfide active site motifs of the enzyme. TTase (GRx) can mimic the catalytic mechanism of TRx in catalysis of ribonucleotide reductase-dependent formation of deoxyribonucleotides (*6*−*8*), and *E. coli* GRx has been studied by NMR in this context (*8*). However, catalysis of reduction of ribonucleotide reductase may not be a general catalytic property of TTase pertinent to all species (*5*). In contrast to TRx, TTase is generally highly selective for glutathione-containing mixed disulfides (e.g., protein-SSG), and its catalytic cycle involves a covalent glutathionyl-enzyme disulfide intermediate (TTase-SSG) rather than an intramolecular disulfide at its active site (*2*, *9*, *10*). Protein-SSG mixed disulfides are a prevalent form of cysteine modification in cells during oxidative stress (*11*−*15*), and TTase likely plays a key catalytic role in redox-regulation of various cellular processes that involve glutathionylated proteins. In particular, there are numerous examples of TTase catalysis of functional reactivation of glutathionylated proteins in vitro, including phosphofructokinase (*16*), HIV-1 protease (*17*), and the transcription factor NFI (*18*).

In the current study, we constructed the quadruple cysteine-substituted mutant of human thioltransferase (C7S, C25S, C78S, C82S), characterized its substrate specificity and kinetic properties, and solved the three-dimensional solution structure of the covalent glutathionyl-enzyme intemediate (QM-TTase-SSG). We chose the quadruple mutant instead of wild-type enzyme for the NMR studies to avoid other nonspecific inter- or intramolecular disulfide bonds besides the C22-S-S-glutathione derivative which is the central intermediate in the TTase catalytic cycle (*2*, *9*, *10*). Moreover, replacement of the other cysteines allowed us to test their participation in determining the specificity and catalytic mechanism of TTase. Comparison of QM-TTase with WT-TTase and the triple mutant (C7S, C78S, C82S) revealed that the Cys-25 moiety that can form the C22-S-S-C25 intramolecular disulfide at the active site detracts from catalysis and is unnecessary for the glutathionyl-disulfide specificity of TTase. These findings contrast with thioredoxin which is inactive without the corresponding second cysteine residue (C35) at the active site. Thus, the 3D structure of QM-TTase-SSG can be interpreted in the context of a specific focus on the glutathionyl specificity and catalytic efficiency of the mutant enzyme. Although the interactions of the glutathionyl moiety with an analogous C14S mutant of *E. coli* glutaredoxin-1 (C14S GRx-C11-SSG) have been addressed previously by NMR (*7*, *19*), human TTase (105 aa) shares only 20% sequence homology with *E. coli* GRx (85 aa), and the human enzyme has additional N-terminal and C-terminal helices (*20*). Moreover, a considerably larger number of NMR restraints have been obtained for the human TTase in this study, which allows a higher resolution structure determination and thus provides more detailed insights into the interactions of the protein with glutathione.

EXPERIMENTAL PROCEDURES

Materials. The vector pET-24d and its host *Escherichia coli* strain BL21(DE3) were obtained from Novagen. T4 DNA polymerase and NADPH were from Boehringer Mannheim. Competent DH5α cells, Isopropyl-β-D-galactopyranoside (IPTG), T4 DNA ligase, calf intestinal alkaline phosphatase (CIAP), T3 promoter primer, T7 promoter primer, and restriction endonucleases were from GibcoBRL. Oligonucleotides 5′-CCTGGAGTACG-3′ and 5′-GGTAAAGATTCTATAGGCGGATCCAGTGATC-3′ were synthesized by the Molecular Biology Core of Case Western Reserve University. 5′-GGCTGCAGGAATGCGACCATGGCTCAAG-3′ and its complementary strand 5′-CCGACGTCCTTACGCTGGTACCGAGTTC-3′ were from Oligos Etc. Qiaex or Qiaex II gel extraction kits were from Qiaex Gene. Quick Change kit for site-directed mutageneses was from Strategene. Wizard Plus Minipreps DNA Purification System and Wizard Maxipreps DNA Purification System were from Promega. Sephadex G50 and Q Sepharose FF were from Pharmacia. Econo-Pac 10DG columns were from Bio-Rad. BCA protein assay reagents were from Pierce. Kanamycin, protamine sulfate, and *E. coli* thioredoxin were from Sigma. Cysteinyl-glutathione disulfide (CSSG) was from Toronto Research Chemicals. $^{15}NH_4Cl$ and [^{13}C]glucose were purchased from Isotec.

Preparation of Mutagenesis Vector for Wild-Type Human Thioltransferase cDNA. PCC-TT2 (*21*) was digested with *Nco*I and treated with DNA polymerase I, large Klenow fragment, to fill in 5′ overhangs. The linear DNA was then cut with *Hin*dIII to release a 0.3 kb fragment containing the cDNA of human TTase. This fragment was gel-purified with Qiaex gel extraction kit as per manufacturer's instructions. pBluescript SK(−) was digested with blunt-end endonuclease *Eco*RV and *Hin*dIII to give a 2.9 kb fragment (the vector) which was gel-purified also. The two fragments were ligated to give pBS-TT3. Listed below are the various primers used for converting four cysteine residues (C7, C25, C78, C82) to serines in human thioltransferase: T3 promoter primer (T3), 5′ ATT AAC CCT CAC TAA AGG GA 3′; T7 promoter primer (T7), 5′ TAA TAC GAC TCA CTA TAG GG 3′; primer A (C7S), 5′ GGA TTT TGG AGT TG 3′; primer B (C25S), 5′ CCT GGA GTA CG 3′; primer C (C78S and C82S), 5′ GGT AAA GAT TCT ATA GGC GGA TCC AGT GAT C 3′; primer D (insert *Nco*I site), 5′ GGC TGC AGG AAT GCG ACC ATG GCT CAA G 3′; primer E (insert *Nco*I site), 5′ CTT GAG CCA TGG TCG CAT TCC TGC AGC C 3′.

Preparation of Triple Mutant Thioltransferase (C7S, C78S, and C82S). TM-TTase was prepared as described by Srinivasan (*22*). Two primers for constructing the triple mutant were synthesized. The forward primer (T3-C7S) was prepared by PCR using pBS-TT3 as template, T3, and primer A. The reverse primer (C78S-C82S-T7) was synthesized by PCR similarly using primer C and T7. The products were gel-purified and subjected to 30 cycles of PCR with T3 and T7 as the primers. This reaction selectively amplified the desired single-strand primers and minimized the concentration of the undesired complementary strand. Then, wild-type TTase template was added to the reaction mixture, and the PCR was continued for 40 cycles. The template for mutagenesis was the gel-purified TTase fragment which was

cut from pBS-TT3 using *Bam*HI and *Hin*dIII so that only the mutagenic primers (T3-C7S and C78S-C82S-T7) could act on the parent strands. Once amplification started, T3 and T7 could join and act on daughter strands. The PCR product (∼0.5 kb) was gel-purified and digested with *Eco*RI and *Hin*dIII and ligated into pBluscript SK(−). The ligation mixture was transformed into competent DH5α *E. coli* cells. The mutation generated a *Bam*HI site within the triple mutant that was used for selection. Those clones that contained the plasmid (pBS-TM) with the *Bam*HI site were DNA-sequenced in both directions to confirm the accuracy of the mutations.

Preparation of Quadruple Mutant Thioltransferase (C7S, C25S, C78S, and C82S). The quadruple mutant was generated from the triple mutant (TM-TTase). Besides its utility for comparative kinetic studies with TM-TTase and WT-TTase, the QM-TTase (C7S, C25S, C78S, C82S) obviated any potential problems for NMR spectroscopy that might arise from oxidative formation of intermolecular disulfide bonds involving these noncatalytic cysteine residues.

Using pBS-TM as the template, T3 and primer B were used to produce the forward primer (T3-C7S-C25S). The T3-C7S-C25S primer was amplified by PCR. Then, both T7 and the template were added to the mixture, and the reaction was allowed to proceed for 40 more cycles. The product (∼0.5 kb) was purified and digested with *Pst*I and *Hin*dIII to give a 0.3 kb fragment that was purified and ligated into similarly digested pBluescript SK vector. The plasmid-containing quadruple mutant (pBS-QM) was confirmed by endonucleotide digestion (lacking *Pst*I site upon mutation of Cys-25 to Ser) and by sequence analysis in both directions.

Construction of Expression Vector for Quadruple Mutant. The Quick-Change kit and primers D and E were used to insert a *Nco*I restriction site at the start codon. The resulting plasmid (pBS-*Nco*I-QM) was subjected to endonuclease digestion and sequence analysis for confirmation. *Nco*I and *Hin*dIII were used to cut out the quadruple mutant cDNA, and it was ligated into the pET-24d expression vector between *Nco*I and *Hin*dIII restriction sites. The plasmid was transformed into competent DH5α *E. coli* as cloning host. A single colony was selected according to endonuclease digestion analysis. The plasmid (pET-QM) isolated from this clone was then transformed into an expression host, *E. coli* strain BL21(DE3). Colonies were screened according to TTase activity.

Expression of ^{13}C and ^{15}N Double-Labeled Quadruple Mutant. Uniformly ^{13}C and ^{15}N double-labeled quadruple mutant TTase was obtained by expression in modified M9 minimal media containing 30 mg of kanamycin, 6 g of [^{13}C]glucose, and 1 g of $^{15}NH_4Cl$. A 25 mL overnight culture was used to inoculate 1 L of minimal media. The cells were grown with shaking at 37 °C at 250 rpm. When bacterial growth reached $A_{600\ nm} = 1.0$, IPTG was added (1 mM final concentration) to induce protein expression, and the culture was continued for 6 h before harvesting by centrifugation at 6000*g* for 15 min. The cell pellet (from 1 L of culture) was resuspended with 20 mL of 10 mM potassium phosphate buffer (pH 7.4), and processed via French press at least twice. The resulting lysate was centrifuged at 48000*g* for 20 min, and the supernatant was evaporated to dryness under vacuum (Savant Speed Vac). The dried crude cell extract was stored at room temperature under vacuum until further use.

Purification of Recombinant [^{13}C, ^{15}N]-QM-TTase. Ten milliliters of 10 mM ammonium formate (pH 5.8), 1 mM DTT was used to reconstitute the dried cell extract from a 1 L bacterial culture. The suspension was centrifuged at 48000*g* for 20 min at 4 °C, and the supernatant was treated with 24 mg/mL protamine sulfate solution to precipitate nucleic acids. About 18 μg of protamine sulfate was added per $A_{260\ nm}$ absorbance unit/cm (total added ca. 100 mg). The resulting protamine sulfate precipitate was centrifuged at 48000*g*, and the supernatant was divided into 1 mL aliquots. Each aliquot was heat-treated in a 60 °C water bath for 1 min; then the recombined sample was centrifuged at 48000*g* and chromatographed on a G50 gel filtration column. Peak fractions containing TTase activity were pooled and passed through a QAE fast flow column. The effluent was collected and dried by Speed Vac. About 6 mg of QM-TTase was obtained from a 1 L culture. The isolated protein was at least 95% pure by HPLC, and the specific activity was about twice that of WT-TTase according to the standard assays of activity (*21*) and protein content (BCA, Pierce). More complete kinetic characterization of QM-TTase relative to WT-TTase is presented under Results and Discussion.

Preparation of the Glutathionyl Mixed Disulfide Adduct of the Quadruple Mutant for NMR Analysis ([^{13}C, ^{15}N]-QM-TTase-SSG). Dried, purified QM-TTase was reconstituted using 50 mM potassium phosphate buffer (pH 6.0) to give a 1 mM solution. An appropriate volume of 20 mM cysteinyl-glutathione was added to give a final concentration of 5 mM. The solution was incubated at 30 °C for 10 min and passed through a 10 mL prepacked desalt column equilibrated with 10 mM potassium phosphate buffer (pH 6.0) to remove excess CSSG and cysteine. The active peak fractions were collected (3 mL total) and concentrated to 0.28 mL by rotary evaporation in vacuo (Speed Vac, Savant). The resulting concentration of thioltransferase was about 1 mM. The glutathionyl mixed disulfide of the ^{15}N-labeled quadruple mutant was subjected to mass spectrometric analysis and gave a molecular mass of 12 027 Da (predicted mass = 12 028 Da; see Results). The final ^{15}N-labeled or $^{15}N/^{13}C$-labeled QM-TTase preparations adducted with unlabeled glutathione were purged with argon and adjusted to 7% ^2H_2O, and transferred to 250 μL microcell NMR tubes (Shigemi Inc., Allison Park, PA) for the experiments described below. Final concentrations of QM-TTase-SSG were ca. 0.9 mM.

NMR Spectroscopy. All the NMR experiments were performed at 25 °C using a Varian Inova 500 MHz spectrometer equipped with a triple-resonance probe head and a shielded *z*-gradient. $^1H-^{15}N$ HSQC and amide hydrogen exchange experiments were recorded on a uniformly ^{15}N-labeled protein (QM-TTase, ca. 1 mM). Sensitivity-enhanced 2D $^1H-^{15}N$ HSQC was collected (*23*) using water-flip-back for water suppression (*24*). Amide hydrogen exchange rates were determined by lyophilizing the protein from ^1H_2O, dissolving the protein in ^2H_2O, and acquiring a series of 2D $^1H-^{15}N$ HSQC spectra at 16 min, 50 min, 80 min, 160 min, 450 min, and 24 h. The sequential assignment of the ^1H, ^{15}N, and ^{13}C chemical shifts was established by means of through-bond heteronuclear correlation spectroscopy along backbone and side chains (*25*, *26*) using 1.0 mM uniformly $^{15}N/^{13}C$-labeled protein, including a series of 3D

triple resonance spectra: HNCACB (*27, 28*), CBCA(CO)-NH (*29*), C(CO)NH (*30, 31*), H(CCO)NH (*31*), and HCCH-TOCSY (*32, 33*). Aromatic resonances were assigned from a 2D clean TOCSY experiment recorded in ^2H_2O, and from $(H_\beta)C_\beta(C_\gamma C_\delta)H_\delta$ and $(H_\beta)C_\beta(C_\gamma C_\delta C_\epsilon)H_\epsilon$ experiments (*34*). The ^{1}H resonances of glutathione were assigned by means of 2D $^{13}C(F_1, F_2)$ doubly filtered HOHAHA (*35*) and $^{13}C-(F_1, F_2)$ doubly filtered NOESY spectra (*36*). An HNHA (*37*) experiment acquired on the uniformly $^{15}N/^{13}C$-double-labeled sample was employed to obtain vicinal $^3J_{HNHA}$ coupling constants that were used for calculating backbone dihedral angle restraints. A 3D $^{15}N/^{13}C$-edited NOESY−HSQC experiment with mixing time of 100 ms was used to derive the intramolecular NOE restraints for structural calculations, while the intermolecular NOE restraints between [^{13}C]-QM-TTase and [^{12}C]glutathione were obtained from a 3D ^{13}C-edited-(F_3)-^{12}C-filtered-(F_2) NOESY experiment with 100 ms of mixing time. The distance restraints were classified semiquantitatively into four distance categories, 1.8−2.7 Å, 1.8−3.5 Å, 1.8−5.0 Å, 1.8−6.0 Å, corresponding to strong, medium, weak, and very weak NOEs, respectively. Upper bond limits involving methyl protons and non-sterospecifically assigned methylene protons were corrected appropriately for center averaging (*38*), and an additional 0.5 Å was added to the upper bound limits involving methyl protons (*39, 40*).

The stereospecific assignments for resonances from non-degenerate β-methylene protons and methyls of Val, Ile, and Leu were obtained by analysis of intraresidue NOE intensities involving NH, $C_\alpha H$, and $C_\beta H$ protons (*41*−*43*). The stereospecific assignments were further confirmed during iterative structure calculations. The ϕ dihedral angle restraints were derived from the coupling constants (HNHA), and χ_1 were derived from the approximate distance restraints for intraresidue and sequential NOE data, and the minimum ranges employed for these angles were $\pm 15°$ and $\pm 20°$, respectively. Slowly exchanging amide protons were identified from a series of 2D $^1H-^{15}N$ HSQC spectra acquired in ^2H_2O, confirming backbone hydrogen bonds deduced from the calculated structure (*44*).

All the data were processed on a Sun UltraSPARC workstation using nmrPipe software (*45*). In the acquisition dimension, all data sets were processed identically. A solvent-suppression filter was applied to the time-domain data, followed by apodization with a 66° shifted squared-sine-bell window, zero-filling to the next power of 2, Fourier transformation, and phasing. The data were apodized in t2 by a 72° shifted sine-bell window prior to zero-filling to 256 complex points, Fourier transformation, and phasing. For HNCACB, CACB(CO)NH, HNHA, C(CO)NH, and H(C-CO)NH, the lengths of the ^{15}N time-domain data were doubled by mirror-image linear prediction, apodized by a squared cosine-bell window, zero-filled to 128 complex points, and Fourier-transformed. The processed spectra were analyzed by the PIPP program (*46*).

Structural Calculations. The structure calculation of QM-TTase-SSG was performed on a SGI INDIGO 2 R10000 workstation using the modified protocol (*47*), which makes use of the program X-PLOR (version 3.2) (*48*). The target function that is minimized during simulated annealing (SA) is comprised of quadratic harmonic potential terms for covalent geometry, square-well quadratic potentials for the experimental distance and torsion angle restraints, harmonic potentials for the $^3J_{HNHA}$ coupling constant (*49*), $^{13}C_\alpha$ and $^{13}C_\beta$ secondary chemical shifts (*50*), and a quadratic van der Waals repulsion term for the nonbonded contacts. No hydrogen-bonding, electrostatic, or 6-12 Lennard−Jones empirical potential energy terms were included in the target function. The initial step of the structure calculation starting from the random coil structure only included unambiguously assigned NOEs and $^3J_{HNHA}$ values. The structures of QM-TTase-SSG were then refined iteratively by assigning the more ambiguous NOEs based on the initial structures. A total of 2658 experimental restraints were used in the final structure calculations, which averages about 25 restraints per residue. These restraints include 2222 NOE distances, 88 ϕ and 64 χ_1 derived from $^3J_{HNHA}$ and stereospecific assignments, respectively, 88 $^3J_{HNHA}$ values, and 102 C_α and 94 C_β secondary shifts. No hydrogen bond constraints were used at any stage of the simulated annealing structure calculations. A total of 95 structures were calculated, among which 70 were well-converged with low energies and no NOE violations >0.3 Å. It should be pointed out that because of the lack of NOE constraints, the carboxylate group of the glutathionyl moiety in the 70 SA structures has 2 conformers: conformer I ($>50\%$) in which the orientation of the carboxylate group forms H-bonds to both S82 NH and S83 NH; and conformer II ($<50\%$) in which the carboxylate group could form a H-bond only to S83 NH. The conformer II was excluded because the S82 NH signal in QM-TTase-SSG is shifted downfield dramatically compared to that in the free QM-TTase form (H-bond evidence, $\Delta\delta = 1.37$ ppm). A set of 20 structures were randomly selected from the conformer I for structural analysis (Table 1).

RESULTS AND DISCUSSION

Properties of the Quadruple Mutant of Human TTase (C7S, C25S, C78S, C82S). Routine analysis of the activity and protein content of the purified QM-TTase revealed a 2-fold higher specific activity (units/mg) compared to WT-TTase under standard assay conditions. Therefore, complete kinetic characterization of QM-TTase was performed in comparison to WT-TTase and TM-TTase (Figure 1). With QM-TTase (at 0.5 mM GSH), both the apparent V_{max} and apparent K_M values for CSSG (upper curve: $V_{max} \cong 3500$ min^{-1}, $K_M \cong 90$ μM) increased about 2-fold relative to WT-TTase. This difference is attributable to the C25S mutation exclusively, because the TM-TTase showed kinetics indistinguishable from WT-TTase (lower curve: $V_{max} \cong 1600$ min^{-1}, $K_M \cong 44$ μM). The identical magnitude of the changes in V_{max} and K_M suggests that the same molecular event is responsible for both changes, and it shows that the catalytic efficiency (V_{max}/K_M) for the disulfide substrate is unchanged relative to WT-TTase.

Figure 2 displays the catalytic cycle for WT-TTase as deduced from previous kinetic and substrate specificity studies (*2, 9, 10*). According to this scheme, the steady-state level of TTase-SSG dictates the overall rate of RSSG reduction, because half-reaction 2 is rate-determining (*10*). Accordingly, the side reaction that depicts reversible formation of TTase-(S-S) intramolecular disulfide (C22-S-S-C25) would detract from the maximal catalytic rate by involving some of the enzyme and GSH in a nonproductive exchange

Table 1: Structural Statistics for TTase-SSG[a]

	⟨SA⟩	$\overline{(SA)}$r
RMSD from exptl distance restraints (Å)		
all (2222)	0.036 ± 0.0006	0.036
sequential ($\|i-j\|=1$) (480)	0.048 ± 0.0013	0.047
medium ($1<\|i-j\|\le 5$) (329)	0.035 ± 0.0024	0.038
long range ($\|i-j\|>5$) (439)	0.019 ± 0.0030	0.013
intraresidue (974)	0.036 ± 0.0008	0.036
RMSD from exptl dihedral restraints (deg) (152)	0.65 ± 0.081	0.69
RMSD from exptl $^3J_{HNa}$ coupling contants (Hz) (88)	0.67 ± 0.055	0.60
RMSD from from exptl ^{13}C shifts		
$^{13}C_\alpha$ (ppm) (102)	1.08 ± 0.037	1.06
$^{13}C_\beta$ (ppm) (94)	0.94 ± 0.043	0.91
RMSD from idealized covalent geometry		
bonds (Å)	0.003 ± 0.0001	0.003
angles (deg)	0.64 ± 0.026	0.65
impropers (deg)	0.51 ± 0.06	0.49
E_{L-J} (kcal mol^{-1})[b]	−411 ± 17	−394
PROCHECK (Ramachandran plot)		
residues in allowed regions (%)	99.8	100
most favored regions (%)	81.5 ± 1.7	80.0
additionally allowed regions (%)	15.2 ± 1.9	16.7
generously allowed regions (%)	3.1 ± 0.8	3.3
disallowed regions (%)	0.2 ± 0.4	0.0
coordinate precision		
RMSD of backbone between ⟨SA⟩ and $\overline{(SA)}$r (Å)[c]	0.25 ± 0.04	
RMSD of heavy atoms between ⟨SA⟩ and $\overline{(SA)}$r (Å)[c]	0.72 ± 0.05	

[a] ⟨*SA*⟩ indicates the ensemble of the 20 simulated annealing structures, (SA) is the mean structure obtained by averaging the coordinates of the individual SA structures best fitted to each other, and $\overline{(SA)}$r is the restrained minimized mean structure obtained by restrained regularization of the mean structure SA. [b] E_{L-J} is the Lennard−Jones van der Waals energy value calculated with the CHARMM empirical energy function and is not included in the target function for SA or restrained minimization. [c] The calculations include glutathione adduct and residues 2−105 for TTase.

reaction. The overall reaction displays a ping-pong pattern of two substrate kinetics. An increase in GSH concentration increases the V_{max} and K_M values for CSSG by the same factor; i.e., the $1/V$ vs $1/[CSSG]$ line is shifted downward in parallel to the original line (*2*, *9*). Removal of the TTase-(S-S) side reaction would lower the intrinsic K_M for GSH, i.e., make GSH more effective at turning over the TTase-SSG intermediate, thus increasing the V_{max} and K_M for CSSG to the same extent, as observed for QM-TTase compared to WT-TTase and TM-TTase (Figure 1). Therefore, with QM-TTase the difference in V_{max} and K_M for CSSG is attributable to the absence of the side reaction, and this should be accompanied by a corresponding decrease in the K_M for GSH. This expectation is documented by the data shown in the inset to Figure 1. Specifically, the double-reciprocal plot shows that the apparent K_M for GSH (at fixed [CSSG]) is decreased whereas the V_{max} is essentially unchanged, consistent with elimination of the side reaction shown in Figure 2. An alternative explanation is conceivable, but less likely. Namely, the Cys-25-SH moiety might participate in stabilization of the TTase-SSG intermediate so that the presence of Cys-25-SH would increase the energy barrier between the TTase-SSG complex and the transition state involving reaction with GSH (i.e., lower V_{max}). Stabilization of TTase-SSG would require less RSSG to maximize TTase-SSG concentration, hence, lower K_M. Effectively the C25S mutant QM-TTase-SSG would lie closer to the transition state

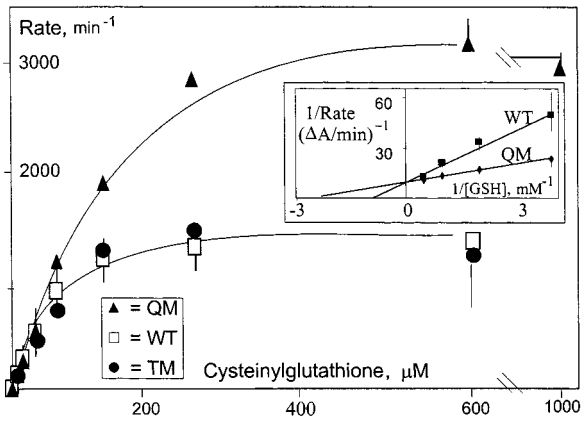

FIGURE 1: Comparative kinetics of mutant and wild-type thioltransferases. Reactions contained 0.2 mM NADPH and 2 units/mL GSSG reductase in 0.1 M potassium phosphate, pH 7.5, in a total volume of 0.2 mL at 30 °C. For the primary graph, GSH concentration was 0.5 mM, and CSSG concentration was varied between 0.025 and 0.2 mM as shown. Open rectangles represent data for WT-TTase, closed circles refer to TM-TTase, and closed triangles correspond to QM-TTase. For the inset, CSSG concentration was 0.1 mM, and GSH concentration was varied between 0.25 and 2.0 mM as shown. Closed rectangles refer to WT-TTase, and closed diamonds refer to QM-TTase. In all cases, 60 ng of TTase protein (WT-, TM-, or QM-TTase) was added to give a final concentration of 25 nM TTase. Apparent K_M and V_{max} values reported in the text were calculated by nonlinear regression analysis of the rate versus concentration relationships. Rates were measured as time-dependent changes in absorbance at 340 nm ($\epsilon = 6.2$ mM^{-1} cm^{-1} for NADPH). The rates of the nonenzymatic reactions were subtracted from the overall rates in the presence of enzyme to give the enzymatic rate in each case, and these differences are the data that are plotted.

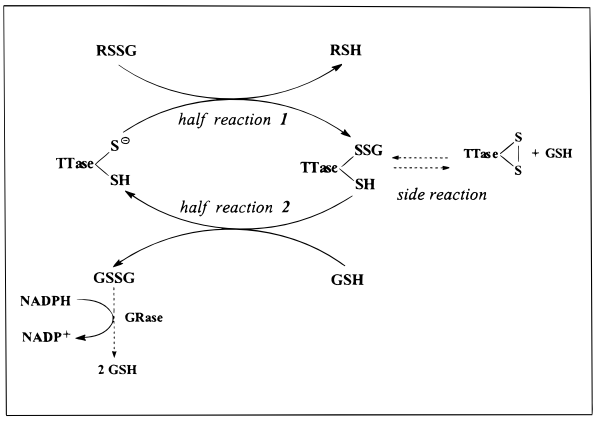

FIGURE 2: Mechanism of thioltransferase catalysis. The central portion of the scheme depicts TTase catalysis of GSH-dependent reduction of a glutathionyl disulfide substrate (RSSG) with concomitant formation of GSSG. TTase is interconverted between thiolate and TTase-SSG forms. At the right is the side reaction involving interconversion of TTase-SSG and the intramolecular disulfide form of TTase (C22-S-S-C25). At the bottom left is the re-formation of GSH by coupling with GSSG reductase.

{TTase-S−GS−SG} than WT-TTase-SSG. Additional mutations of the C25 residue could address this possibility.

Other characteristics of WT-TTase were also compared to those of QM-TTase. First, the specificity of the mutant enzyme was tested by assaying its ability to catalyze GSH-dependent dethiolation of [^{35}S]-BSA−SSG and [^{14}C]-BSA−SS-cysteine. This experiment addressed the fundamental question whether the Cys-25-SH moiety could be responsible for the enzyme's ability to discriminate between glutathione-

containing (e.g., BSA−SSG) and non-glutathione-containing (e.g., BSA−SS-Cys) mixed disulfide substrates. Like WT-TTase, the mutant enzyme QM-TTase effectively catalyzed release of radioactivity from BSA−SSG (turnover = 344 min^{-1}) under standard assay conditions (*21*). No catalysis of BSA−SS-cysteine ^{14}C dethiolation was observed even with 100-fold more enzyme. Thus, the specificity of TTase for glutathionyl disulfide substrates is clearly retained by the mutant lacking the cysteine-25 moiety. This result refutes the hypothesis that more extensive nonproductive cycling between TTase-S-SR and TTase-(S-S) forms, promoted by non-glutathionyl disulfides (R′SSR), could be the exclusive basis for the enzyme's preference for glutathionyl disulfide substrates (*2*). More likely the enzyme facilitates formation of the TTase-SSG intermediate by providing specific molecular interactions between residues on the enzyme and components of the adducted glutathionyl moiety. The NMR structural data below are consistent with this hypothesis. Selective glutathionyl accommodation is also supported by the observation that reaction of QM-TTase with CSSG gives QM-TTase-SSG exclusively (see below). However, there are paradoxical data that suggest that the glutathionyl specificity of TTase cannot be interpreted simply by the typical concept of a reversible noncovalent binding site for the glutathione moiety (*2*). For example, we found no binding of reduced thioltransferase to an affinity column in which GSH in its reduced form is attached to a spacer arm. In contrast, glutathione-*S*-transferase binds avidly to this type of column. Moreover, neither *S*-methylglutathione nor *S*-nitrosoglutathione (up to 5 mM) appears to be an inhibitor of human thioltransferase, although *p*-nitrophenyl-*S*-glutathione does inhibit somewhat (*22*), and Hoog et al. reported competitive inhibition of *E. coli* glutaredoxin by other aromatic *S*-substituted glutathione analogues (*51*).

Characterization of QM-TTase-SSG. We studied formation of QM-TTase-SSG by reaction with CSSG in the absence of GSH, because CSSG is the prototype disulfide substrate for the standard spectrometric assay of TTase (*21*), and this approach provided an opportunity to scrutinize the substrate specificity in a nonturnover situation. Remarkably, QM-TTase-SSG is formed virtually exclusively from the reaction of QM-TTase with CSSG (Figure 3). QM-TTase was prepared, purified, and reacted with CSSG as described under Experimental Procedures. The reaction mixture gave only one protein band upon HPLC purification, and this was subjected to mass spectral analysis. The mass spectrum (Figure 3) gave a series of related *m*/*z* peaks reflective of a single species with a molecular mass of 11 883 ± 3 Da (molecular mass predicted for QM-TTase-SSG = 11 885 Da). ^{15}N-labeled QM-TTase-SSG was also examined by mass spectral analysis on a Finnigan Quadrupole Electrospray mass spectrometer [mass predicted 12 028 Da; mass observed 12 027 Da (spectrum not shown)].

The exclusive formation of QM-TTase-SSG is unusual since the S−S bond in CSSG is not expected to be so polarized to favor such a selective attack. More likely this reflects stabilization of the incipient TTase-SSG adduct relative to TTase-SSCys. The high-resolution structure of the TTase-SSG intermediate by multidimensional NMR spectroscopy clearly demonstrates the specific molecular interactions of TTase with the glutathionyl moiety (below).

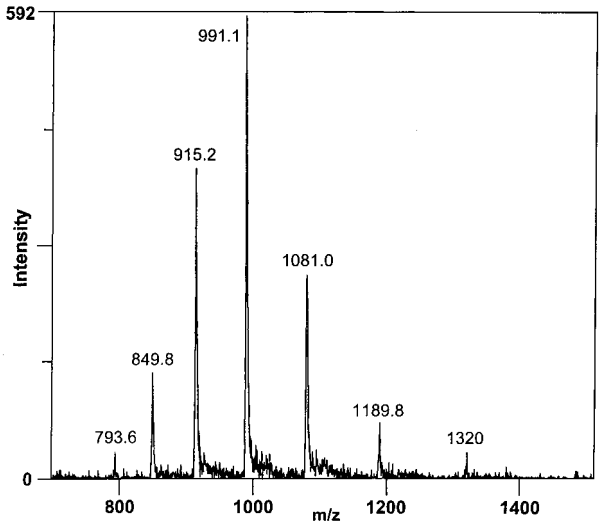

FIGURE 3: Mass spectrum of QM-TTase-SSG, product of CSSG reaction with QM-TTase. Quadruple mutant TTase was prepared, purified, and reacted with cysteinyl-glutathione disulfide as described under Experimental Procedures. The reaction mixture was repurified by HPLC to separate small molecules. Only one protein band appeared on the HPLC, and this was subjected to mass spectral analysis. The spectrum above was obtained from a 20 μL injection of QM-TTase (5 μM according to protein assay) into the Extel Benchmark electrospray mass spectrometer. Consistent with the single band on the HPLC, only one species was evident in the mass spectrum. The spectrum was deconvoluted by converting the *m*/*z* values of the array of peaks to mass values. A single mass value was obtained from every *m*/*z* peak, namely, 11 883 ± 3 Da. The calculated value for QM-TTase-SSG is 11 885 Da.

Sequential NMR Resonance Assignments. Figure 4 shows the $^1H-^{15}N$ HSQC spectrum for the uniformly ^{15}N-labeled quadruple mutant (C7S, C25S, C78S, C82S) of human TTase (105 aa) in the disulfide adduct with glutathione at C22. The spectrum displays good chemical shift dispersion in both ^1H and ^{15}N dimensions, although there are 10 overlapping pairs of $^1H-^{15}N$ cross-peaks out of 100 non-proline residues, which include F4/L85, R27/D77, I31/L41, L32/T53, L41/L94, I47/D58, N54/L60, E55/R71, I74/K99, K76/Q89, and S78/S83.

Assignments of the backbone ^1H, ^{13}C, and ^{15}N resonances were made using the standard procedure (*25*), which relies on the complementary HNCACB and CBCA(CO)NH through-bond correlation experiments. Briefly, the HNCACB experiment correlates the amide resonances with both intraresidue $^{13}C_\alpha$ and $^{13}C_\beta$ resonances and preceding interresidue $^{13}C_\alpha$ and $^{13}C_\beta$ resonances, whereas the CBCA(CO)NH experiment only connects amide resonances and the preceding interresidue $^{13}C_\alpha$ and $^{13}C_\beta$ resonances. Virtually complete backbone assignments except for prolines were made based on the combination of these two experiments. H_α resonances were then assigned based on a 3D HNHA experiment, in which 88 out of 100 non-proline residues displayed $NH-H_\alpha$ *J*-correlations.

The side-chain resonances were obtained by the combined analysis of HCCH-TOCSY, ^{15}N-edited HOHAHA, C(CO)-NH, and H(CCO)NH experiments, which provide H_j-$^{13}C_j$-$^{13}C_{j\pm n}$-$H_{j\pm n}$, $H_j(i)$-$^{15}N(i)$-$NH(i)$, $^{13}C_j(i-1)$-$^{15}N(i)$-$NH(i)$, and $H_j(i-1)$-$^{15}N(i)$-$NH(i)$ correlations, respectively. The assignments of the side chains further confirmed the backbone assignments derived from HNCACB and CBCACONH. Aromatic resonances were assigned from a combination of

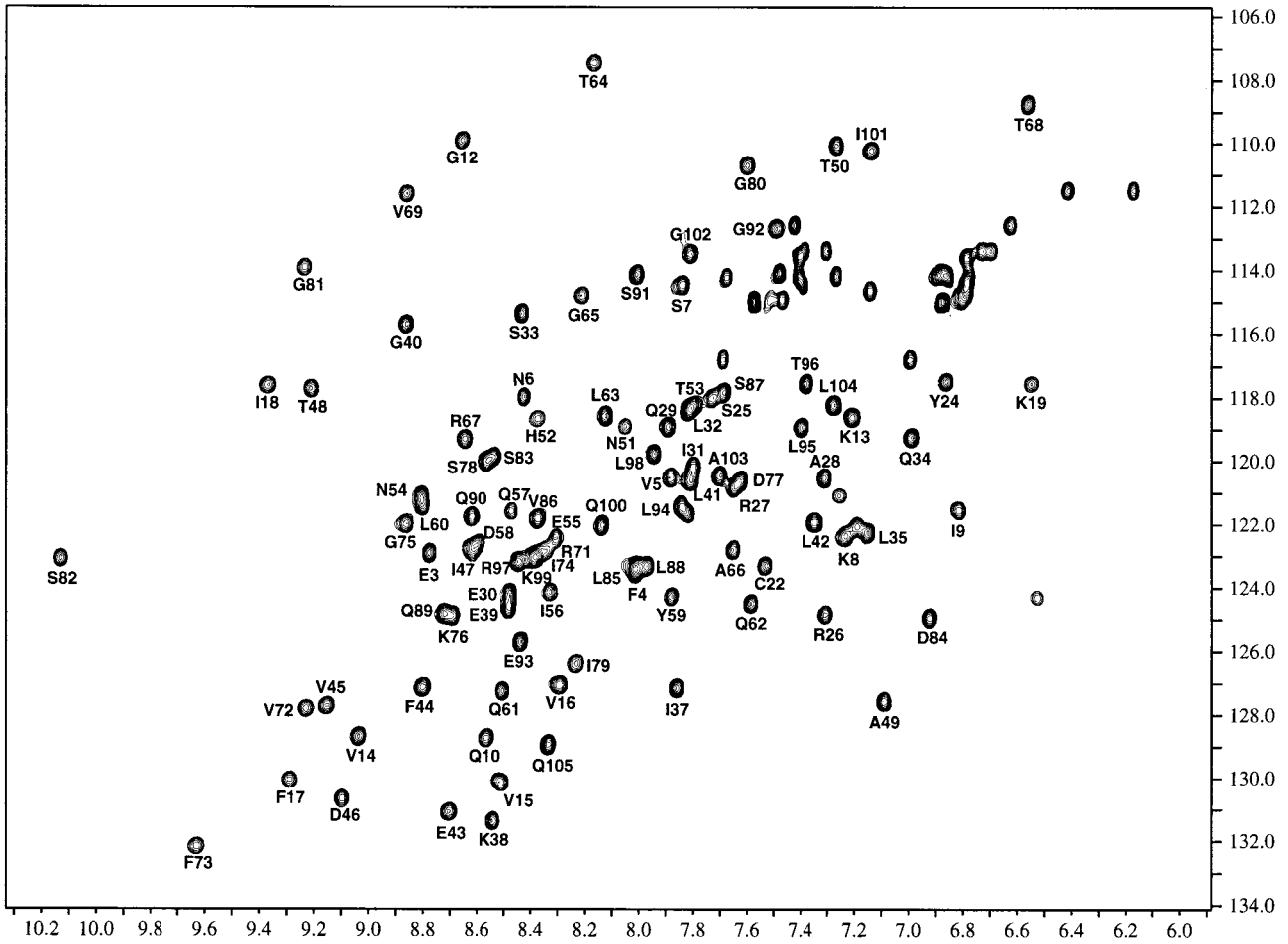

FIGURE 4: Two-dimensional $^1H-^{15}N$ HSQC spectrum of human QM-TTase-SSG at pH 6.0, 25 °C.

a 2D clean TOCSY experiment and $(H_\beta)C_\beta(C_\gamma C_\delta)H_\delta$ and $(H_\beta)C_\beta(C_\gamma C_\delta C_\epsilon)H_\epsilon$ experiments. The latter two experiments provide direct correlations between the resonances of C_β and protons of aromatic rings. The 2D-TOCSY was used to examine the spin systems of aromatic rings. The aromatic assignments were further confirmed by checking NOE connectivities between aromatic protons to the backbone protons using a 3D $^{15}N/^{13}C$-edited NOESY experiment. Once completed, assignments for each residue were also checked on the basis of sequential NOE connectivities observed in the NOESY spectrum.

Secondary Structure. Figure 5 summarizes the amide proton exchange data, the short- and medium-range NOE data involving amides obtained from the 3D $^{15}N/^{13}C$-NOESY−HSQC spectrum, the $^3J_{HNHA}$ values calculated from the HNHA spectrum, and the deviations from random-coil values of the C_α and C_β chemical shifts (*52*, *53*). The secondary structural elements, as inferred from the above data, are indicated in Figure 5 as well. The regular secondary structures of the protein (64% of the sequence) comprise five α-helices including Q2−K8, P23−S33, T53−T64, S82−Q90, and E93−I101, and four β-strands including K13−I18, L42−I47, P70−I74, and D77−G80. The four β-strands in QM-TTase-SSG form a four-stranded β-sheet topology. Our data are consistent with the recent crystal structure of the oxidized form of pig liver thioltransferase (80% sequence homology; see ref *20*). The four-stranded β-sheet topology of QM-TTase-SSG also agreed with that reported for unadducted wild-type human thioltransferase (*54*); however, the lengths of the first (4−10) and last (93−103) α-helices in the wild-type TTase reported by Sun et al. (*54*) are different from those for the QM-TTase-SSG and pig-liver TTase, which are 2−8 and 93−101, respectively.

Structure Determination. The structure calculations were performed iteratively using the procedures as described in (*55*) for the structures of thioredoxin in mixed disulfide complex with the NFkB target peptide. The stereoview of a best-fit superposition of the backbone (C_α trace) for a set of 20 SA structures is shown in Figure 6 (see Table 1 for statistics). The structure of QM-TTase-SSG is well-defined, except for the loop region which connects β2 and α3. This region is exposed to the protein surface, which appears to be flexible and exhibit fewer NOE connectivities. The average rms difference between the 20 SA structures and the mean coordinates is 0.25 Å for backbone atoms and 0.72 Å for all atoms, respectively, with no distance violations greater than 0.3 Å and no dihedral angle violations greater than 5° (Table 1). The resolution of the solution structure of QM-TTase-SSG is high, which allows a detailed structure−function analysis of the protein.

Description of the QM-TTase-SSG Structure. The overall structure of QM-TTase in the glutathionyl complex (Figure 7) is characteristic of a four-stranded mixed β-sheet (residues 13−18, 42−47, 70−74, and 77−80) surrounded by five α-helices (residues 2−8, 23−34, 53−64, 82−90, and 93−101). The strands β2, β3, and β4 are antiparallel, whereas β1 and β2 are parallel. The β-sheet is flanked on one side by three helices, α2, α4, and α5, and on the opposite side

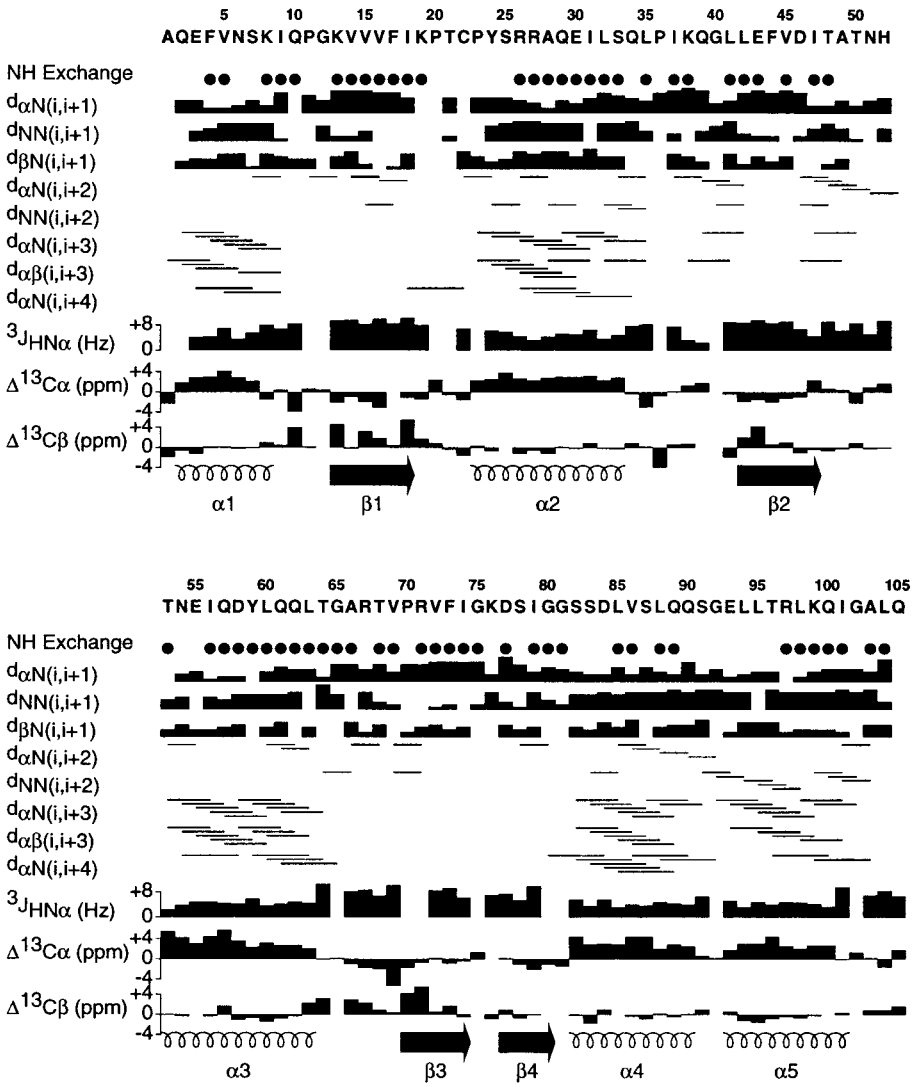

FIGURE 5: Summary of the NMR data obtained for QM-TTase-SSG on NH exchange, sequential and medium-range NOEs involving NH, $C_\alpha H$, $^3J_{HNHA}$ coupling constants, C_α and C_β secondary shifts, and the secondary structure deduced from these data. NH exchange: filled circles indicate $^{15}N-^1H$ correlations subject to slow hydrogen exchange. NOEs: the height of the bar indicates the strength of the NOE. $^3J_{HNHA}$ coupling constants: the height of the bar reflects the values obtained from the HNHA experiment (*37*).

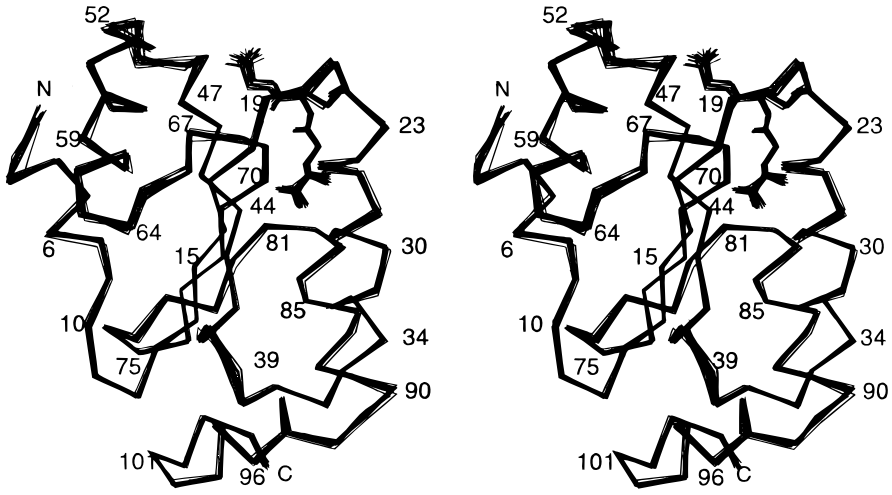

FIGURE 6: Solution structure of QM-TTase-SSG. Stereoview showing a best-fit superposition of a backbone C_α trace of a set of 20 simulated annealing structures. The structures are well-defined except for the loop linking the strand-β2 and helix-α3. The statistics of the structures are shown in Table 1.

by helices α1 and α3. α2 and α4 are parallel to each other and to the sheet, whereas α3 stretches across the sheet. α1 and α5 are additional helices in human TTase compared to *E. coli* GRx, and they pack against α3 and α4, respectively.

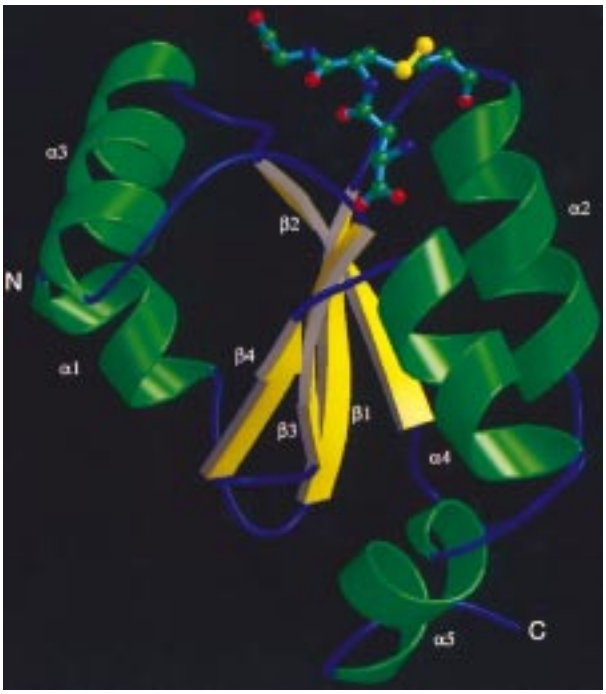

FIGURE 7: Ribbon representation of the QM-TTase-SSG structure. All the α-helices and β-strands are labeled sequentially, i.e., α1 to α5 and β1 to β4. The adducted glutathionyl moiety is shown in ball-and-stick mode. The figure was prepared with the program MOLSCRIPT (*58*).

The main tertiary interactions in the structure of TTase can be described by two large clusters, which primarily involve hydrophobic residues from the β-sheet and α-helices. The two clusters are located on either side of the central sheet that contributes significantly to the stabilization of the protein structure. Cluster 1 mainly contains a hydrophobic core involving F4, V5, and the hydrophobic part of K8 from α1; I56, L60, L63, and hydrophobic parts of T53, Q57, Y59, and T64 from α3; V15, F17, V45, F73, and the hydrophobic part of R71 from the central β-sheet; and I9, I47, V69 and the hydrophobic part of K19 and T48 from the loop. Cluster 2, which is located on the other side of the β-sheet, contains a hydrophobic core involving A28, I31, L32 from α2; L85, L88 from α4; L94, L95, L98, I101, and the hydrophobic part of R97 from α5; V14, V16, I18, L42, F44, P70, V72, I74, I79 from the central β-sheet and the loop residues L35, I37, L41, V69, and A103. In addition to the hydrophobic interactions, the structure calculations indicate that most of the hydrophilic residues in the above two clusters are involved in hydrogen bonding or electrostatic interactions, which play an important role in stabilization of the tertiary packing of the enzyme and its interaction with the bound glutathione moiety. For example, although the hydrophobic parts of K19, Q57, and R71 are involved in hydrophobic interactions in cluster 1, their hydrophilic parts appear to hydrogen-bond or salt-bridge with the adducted glutathionyl moiety (see below). Other hydrogen bonds or salt bridges involving hydrophilic residues of the two clusters as revealed from the structure are the K13 NH_3^+ group with the carbonyl oxygen of G40, the hydroxyl group of Y59 with the carbonyl group of I6, the K76 NH_3^+ group with the carbonyl group of I9, and the guanidinium group of R97 with the carboxylate group of D77 and the side chain carbonyl oxygen of Q100.

All the deduced hydrogen bonding patterns involving backbone atoms of the protein are consistent with the expected geometry and amide proton exchange data. It is interesting that some loop/turn regions are well-defined and stabilized by hydrogen bond interactions. For example, consistent with its slow amide exchange behavior, the loop T64−V69 region reveals two hydrogen bond pairs within the protein: T64HN−L60O and G65HN−T64O. In addition, this loop region interacts with the bound glutathionyl moiety by having hydrogen bonds between V69 HN and carbonyl groups of the γ-glutamate and Cys residue of glutathione, and between the R67 side chain and glycinyl carboxyl group of glutathione, respectively (see the section below). Hydrogen bonds were also identified in the loop region between β2 and α2, including L35HN−L32O, I37HN−L35O, and K38HN−A103O pairs. The C-terminal loop (G102−Q105) also contains hydrogen bond pairs Q105HN−P36O, A103HN−L98O, and A103O−K38HN.

The Glutathionyl Interaction Site. The detailed interaction of the glutathionyl moiety with the TTase protein is shown in Figure 8, in which the glutathionyl moiety displays an extended conformation and is localized in a cleft on the protein surface. The cleft is formed by the residues from helix-α2 (P23, Y24, S25), helix-α3 (S82, S83), the β3 strand (P70, R71), the active-site loop (K19, P20, T21, C22), and the loop (R67, T68, V69) that connects helix-α3 and strand-β3 (Figure 8). The disulfide bridge between Cys-22 of QM-TTase and Cys-2′ of glutathione has a right-handed trans-trans-gauche(−)-trans-gauche(−) conformation with a $C_\alpha-C_\alpha$ separation of 6.85 Å, similar to that of the disulfides that span the β-barrels in immunoglobulins (*55*), with trans-gauche-trans (180°, ±90°, 180°) conformation in χ_2, χ_3, χ_2' and 6.6−7.4 Å of $C_\alpha-C_\alpha$ separation. Figure 9 shows a schematic diagram of the interactions between the TTase protein and the glutathione adduct. In addition to the covalent linkage afforded by the disulfide bridge, numerous noncovalent interactions between the glutathione and QM-TTase were also identified, including van der Waals contacts, hydrogen bonding, and salt bridges. The residues involved in van der Waals interactions with the glutathione are Y24, S25, T68, V69, and P70, respectively (Figure 9). The carboxylate group of the glutathionyl Gly residue likely hydrogen-bonds to the side chain amide group of Q57 and salt-bridges with the R67 guanidinium group and the K19 NH_3^+ group, respectively (Figure 9). The carbonyl groups of the γ-glutamate and the Cys residues of the glutathionyl moiety of QM-TTase-SSG both hydrogen-bond to V69 NH, which is consistent with the significantly downfield shifted V69 NH and with the fact that V69 NH exchanges slowly with water in the complex but fast in the free form (QM-TTase) (data not shown). The carboxylate group of the glutathionyl γ-glutamate forms a salt bridge with the R71 guanidinium group and also hydrogen-bonds to the backbone amides of S82 and S83 that are significantly downfield shifted in QM-TTase-SSG compared to QM-TTase, although the exchange rates of these two amides are too fast to be measured on the NMR time scale (data not shown). Some electrostatic interactions may also occur between the negatively charged carboxylate group of the γ-glutamate and the nearby partially postively charged N-terminal end of the helix-α4 dipole (*57*). It should be emphasized that although no direct NOE data are available for hydrogen bonds and

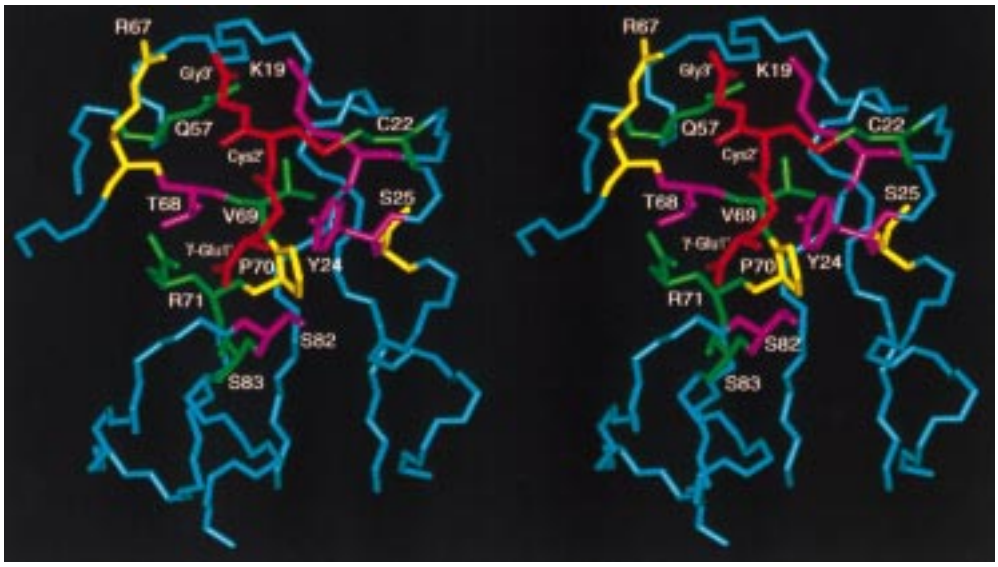

FIGURE 8: Stereoview of the backbone trace of QM-TTase-SSG with the active site residues highlighted. The adducted glutathionyl moiety is colored in red. The side chains which interact with the adducted glutathione are S25, R67, and P70 (colored in yellow, respectively); C22, Q57, V69, R71, and S83 (colored in green, respectively); and K19, Y24, T68, and S82 (colored in pink, respectively).

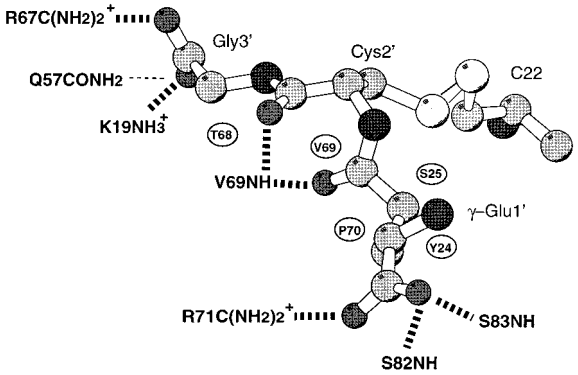

FIGURE 9: Schematic representation showing interactions between the TTase protein and adducted glutathione. The hydrogen bonds and salt briges deduced from the calculated structures are illustrated with the dashed lines (thick dashed line). All the hydrogen bonds and salt bridges were present in more than 50% of the 20 SA structures except Q57-GSH (35%, shown by thin dashed line). The 5 residues of TTase involved in 31 intermolecular van der Waals contacts with the glutathione moiety are shown by circles.

salt bridges as described above, these conclusions were derived from a significant percentage of the 20 SA structures (>50%), and many of them are supported by slow amide exchange and chemical shift data as described above (Figure 9).

Structural Comparison with Other Thioltransferases. (a) QM-TTase-SSG vs Crystal Structure of Pig Liver TTase. Figure 10A shows the best fit of superposition of the restrained minimized mean structure of human QM-TTase-SSG and the X-ray crystal structure of the oxidized form of pig liver TTase, which share ~80% sequence homology. The overall structures of the two proteins are very similar with the rms difference of the backbone (C, C_α, N, O) atoms being 1.09 Å for residues 2−105. The β-bulge opposite to the conserved cis Pro-70 observed in pig liver TTase is also present in human TTase. The side chains of the active site residues, which are largely exposed to the surface in the unligated structure of pig liver TTase (*20*), are involved in electrostatic and van der Waals interactions in the NMR structure of the QM-TTase-SSG complex. As a result of the glutathione adduct, the loop comprising G65-A66-R67-T68-V69-P70 in the NMR structure of the complex appears to move slightly toward the direction of helices-α2, as compared to the unligated structure of pig liver TTase (Figure 10A). Besides the loop region, the C-terminal helix-α5 region between QM-TTase-SSG and pig liver TTase also displays larger-than-average differences (Figure 10A). Interestingly, this region is missing in the *E. coli* GRx and may be structurally important for the function of mammalian TTase (see below).

(b) NMR Structure of Human QM-TTase-SSG vs E. coli GRx-SSG. Human TTase and *E. coli* Grx share ~20% sequence homology, with the former having N-terminal and C-terminal helices. Best-fit superposition of the minimized average NMR structure of QM-TTase-SSG and the NMR structure of *E. coli* glutaredoxin (C14S) with glutathione (GRx-SSG) (*19*) is shown in Figure 10B. The overall folding topology including the active site is similar for the two proteins, i.e., four-stranded β-sheet flanked by similarly oriented α-helices. Although the two additional N-terminal and C-terminal helices are distant from the active site in human TTase, they pack tightly with other helices and may play some role in structural stabilization and function. The interactions of the glutathionyl moiety at the active sites of both proteins are largely similar; however, a detailed comparison between the two protein complexes reveals some important differences: (1) The Gly carboxylate group of the GS moiety in QM-TTase-SSG makes salt bridges to the guanidinium group of R67 and the NH_3^+ group of K19 and it hydrogen-bonds to the side chain amide of Q57, whereas in *E. coli* GRx-SSG this group only makes one salt bridge to the NH_3^+ group of K45. (2) The backbone amide proton of V69 in QM-TTase-SSG hydrogen-bonds to the carbonyl oxygens of both γ-glutamate and Cys residues of the glutathione whereas the corresponding V59 in *E. coli* GRx-SSG only hydrogen-bonds to the carbonyl oxygen of the glutathionyl Cys residue. It is important to point out that >90% of the calculated structures show the H-bond between γ-glutamate CO and V69 NH. (3) None of the calculated structures for QM-TTase-SSG exhibit a salt bridge between

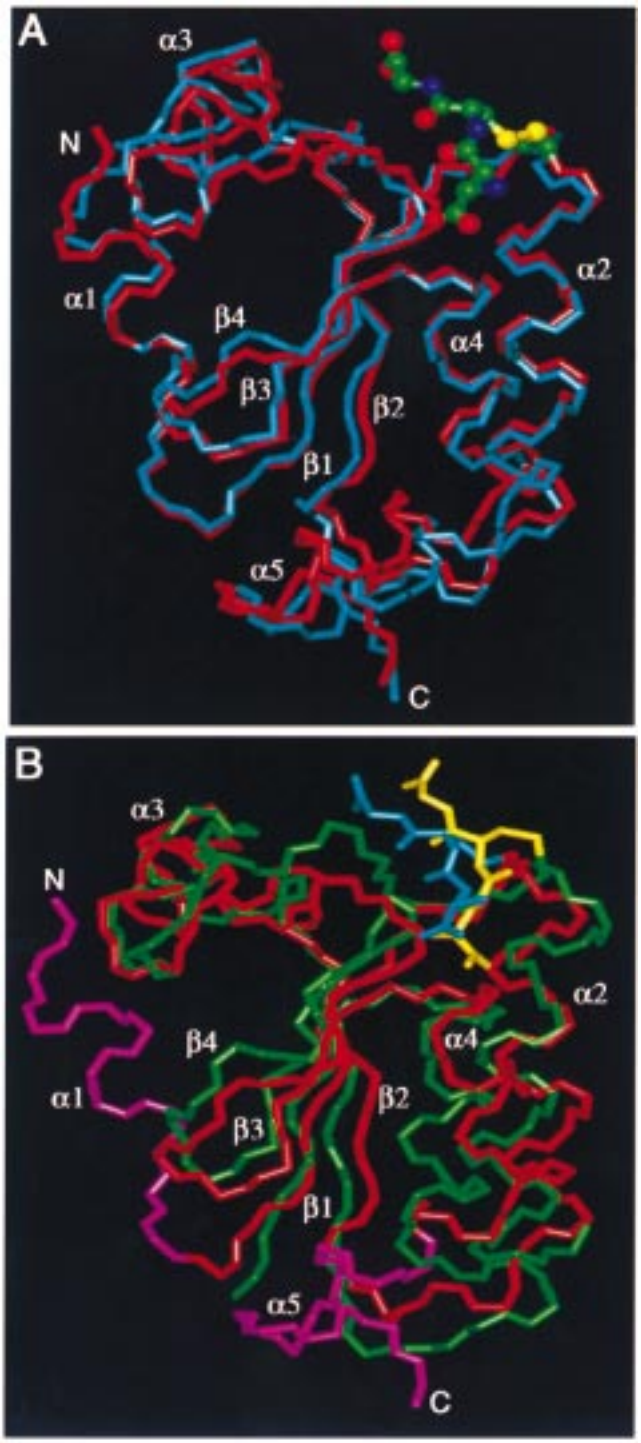

FIGURE 10: (A) Backbone overlay of human QM-TTase-SSG (red) and the crystal structure of pig liver TTase (blue). The glutathione moiety in QM-TTase-SSG is shown in the ball-and-stick mode. (B) Backbone overlap of human QM-TTase-SSG (red) and the NMR structure of *E.coli* (C14S) GRx-SSG (green). The glutathione moiety is colored in blue for the human TTase-SSG and in yellow for the *E. coli* GRx-SSG.

the NH_3^+ group of γ-glutamate and the carboxylate group of conserved D84 (corresponding to D74 in *E. coli* Grx), which was suggested for the *E. coli* GRx-SSG structure. In fact, an NH_3^+ signal for γ-glutamate was not observable by NMR probably due to its fast exchange with water. On one hand, these differences in electrostatic interactions may reflect subtle differences in stabilization of the respective glutathionyl adduct of *E. coli* GRx and human QM-TTase, which only share ~20% sequence homology. On the other hand, the differences may result from the relative resolution of the calculated NMR structures. We are designing new site-directed mutagenesis and kinetic studies along with NMR experiments to evaluate the contributions of the residues of TTase implicated in stabilizing the TTase-SSG intermediate. These studies will provide further insights regarding the basis for the glutathionyl specificity of TTase in both steps of its catalytic mechanism (*2*, *10*).

CONCLUDING REMARKS

We have determined the high resolution structure of the quadruple Cys to Ser mutant of human TTase (C7S, C25S, C78S, C82S) in the mixed disulfide intermediate complex with glutathione. The structure reveals numerous van der Waals and electrostatic interactions between TTase and the glutathionyl moiety and provides detailed atomic insights regarding the structural basis of TTase specificity for glutathione-containing mixed disulfide substrates. The quadruple mutant that retains only the active site cysteine residue (C22) displays the same specificity for protein-SSG substrates and enhanced catalysis relative to wild type TTase and the triple mutant (C7S, C78S, C82S), indicating that the Cys-25-SH moiety is not required for catalysis or specificity. These findings contrast with thioredoxin which is inactive without the corresponding second cysteine residue (C35) at its active site. Overall, the results indicate that TTase operates via a distinct catalytic pathway in specifically reducing protein-S−S-glutathione mixed disulfides that occur during oxidative stress or as redox intermediates in signal transduction.

ACKNOWLEDGMENT

We thank Usha Srinivasan, Carol Chrestensen, and Sarah Younkin for constructing the triple mutant vector, and we thank Carol Chrestensen, Laura Donlin, and Usha Srinivasan for help in construction of the quadruple mutant. We are grateful to Paul Minkler and Michael Goshe for performing mass spectral analyses. We also thank Frank Delaglio and Dan Garrett for nmrPipe and Pipp software.

REFERENCES

1. Holmgren, A. (1989) *J. Biol. Chem. 264*, 13963−13966.
2. Mieyal, J. J., Gravina, S. A., Mieyal, P. A., Srinivasan, U., and Starke, D. W. (1995) in *Biothiols in Health and Disease* (Packer, L., and Cadenas, E., Eds.) Part A, Chapter 14, pp 305−372, Marcel Decker, Inc., New York.
3. Powis, G., Gasdaska, J. R., and Baker, A. (1997) *Adv. Pharmacol. 38*, 329−359.
4. Nakamura, H., Nakamura, K., and Yodoi, J. (1997) *Annu. Rev. Immunol. 15*, 351−369.
5. Wells, W. W., Yang, Y., Deits, T. L., and Gan, Z. R. (1993) *Adv. Enzymol. Relat. Areas Mol. Biol. 66*, 149−201.
6. Luthman, M., and Holmgren, A. (1982) *J. Biol. Chem. 257*, 6686−6690.
7. Bushweller, J. H., Aslund, F., Wüthrich, K., and Holmgren, A. (1992) *Biochemistry 31*, 9288−9293.
8. Berardi, M. J., Pendred, C. L., and Bushweller, J. H. (1998) *Biochemistry 37*, 5849−5857.
9. Gravina, S. A., and Mieyal, J. J. (1993) *Biochemistry 32*, 3368−3376.
10. Srinivasan, U., Mieyal, P. A., and Mieyal, J. J. (1997) *Biochemistry 36*, 3199−3206.
11. Chai, Y. C., Hendrich, S., and Thomas, J. A. (1994) *Arch. Biochem. Biophys. 310*, 264−272.

12. Rokutan, K., Johnston, R. B., Jr., and Kawai, K. (1994) *Am. J. Physiol. 266(2 Pt. 1)*, G247−G254.
13. Rahman, I., Li, X. Y., Donaldson, K., Harrison, D. J., and MacNee, W. (1995) *Am. J. Physiol. 269(3 Pt. 1)*, L285−L292.
14. Ciriolo, M. R., Palamara, A. T., Incerpi, S., Lafavia, E., Bue, M. C., De Vito, P., Garaci, E., and Rotilio, G. (1997) *J. Biol. Chem. 272*, 2700−2708.
15. Cohen, G., Farooqui, R., and Kesler, N. (1997) *Proc. Natl. Acad. Sci. U.S.A. 94*, 4890−4894.
16. Yoshitake, S., Nanri, H., Fernando, M. R., and Minakami, S. (1994) *J. Biochem. 116*, 42−46.
17. Davis, D. A., Newcomb, F. M., Starke, D. W., Ott, D. E., Mieyal, J. J., and Yarchoan, R. (1997) *J. Biol. Chem. 272*, 25935−25940.
18. Bandyopadhyay, S., Starke, D. W., Mieyal, J. J., and Gronostajski, R. M. (1998) *J. Biol. Chem. 273*, 392−397.
19. Bushweller, J. H., Billeter, M., Holmgren, A., and Wüthrich, K. (1994) *J. Mol. Biol. 235*, 1585−1597.
20. Katti, S. K., Robbins, A. H., Yang, Y., and Wells, W. W. (1995) *Protein Sci. 4*, 1998−2005.
21. Chrestensen, C. A., Eckman, C. B., Starke, D. W., and Mieyal, J. J. (1995) *FEBS Lett. 374*, *1*, 25−28.
22. Srinivasan, U. (1998) Ph.D. Thesis, Department of Chemistry, Case Western Reserve University, Cleveland, OH.
23. Kay, L. E., Keifer, P., and Saarinen, T. (1992) *J. Am. Chem. Soc. 114*, 10663−10665.
24. Grzesiek, S., and Bax, A. (1993) *J. Am. Chem. Soc. 115*, 12593−12594.
25. Bax, A., and Grzesiek, S. (1993) *Acc. Chem. Res. 26*, 131−138.
26. Clore, G. M., and Gronenborn, A. M. (1991) *Science 252*, 1390−1399.
27. Wittekind, M., and Muller, L. (1993) *J. Magn. Reson. B 101*, 201−205.
28. Muhandiran, D. R., and Kay, L. E. (1994) *J. Magn. Reson. B 103*, 203−216.
29. Bax, A., and Grzesiek, S. (1992) *J. Am. Chem. Soc. 114*, 6291−6293.
30. Grzesiek, S., Anglister, J., and Bax, A. (1993) *J. Magn. Reson. Ser. B 101*, 114−119.
31. Logan, T. M., Olejniczak, E. T., Xu, R. X., and Fesik, S. W. (1992) *FEBS Lett. 314*, 413−418.
32. Bax, A., Clore, G. M., Driscoll, P. C., Gronenborn, A. M., Ikura, M., and Kay, L. E. (1990*) J. Magn. Reson. 87*, 620−627.
33. Kay, L. E., Xu, G.-Y., Singer, A. U., Muhandiram, D. R., and Forman-Kay, J. D. (1993) *J. Magn. Reson. B 101*, 333−337.
34. Yamazaki, T., Forman-Kay, J. D., and Kay, L. (1993) *J. Am. Chem. Soc. 115*, 11054−11055.
35. Bax, A., Grzesiek, S., Gronenborn, A. M., and Clore, G. M., (1994) *J. Magn. Reson. B 106*, 269−273.
36. Lee, W., Revington, M. J., Arrowsmith, C., and Kay, L. E., (1994) *FEBS Lett. 350*, 87−90.
37. Vuister, G. W., and Bax, A. (1993) *J. Am. Chem. Soc. 115*, 7772−7777.
38. Clore, G. M., Gronenborn, A. M., Nilges, M., and Ryan, C. A. (1987) *Biochemistry 26*, 8012−8013.
39. Wagner, G., Braun, W., Havel, T. F., Schaumann, T., Go, N., and Wüthrich, K. (1987) *J. Mol. Biol. 196*, 611−639.
40. Powers, R., Garrett, D. S., March, C. J., Frieden, E. A., Gronenborn, A. M., and Clore, G. M. (1993) *Biochemistry 32*, 6744−6762.
41. Arseniev, A., Schultze, P., Wörgötter, E., Braun, W., Wagner, G., Vasàk, M., Kägi, J. H. R., and Wüthrich, K. (1998) *J. Mol. Biol. 201*, 637−657.
42. Hybert, S. G., Karki, W., and Wagner, G. (1987) *EMBO J. 164*, 625−635.
43. Zuiderweg, E. R. P., Boelens, R., and Kaptein, R. (1985) *Biochemistry 24*, 601−611.
44. Wüthrich, K. (1986) *NMR of proteins and nucleic acids*, John Wiley & Sons, New York.
45. Delaglio, F., Grzesiek, S., Vuister, G. W., Zhu, G., Pfeifer, J., and Bax, A. (1995) *J. Biomol. NMR 6*, 277−293.
46. Garrett, D. S., Powers, R., Gronenborn, A. M., and Clore, G. M. (1991) *J. Magn. Reson. 95*, 214−220.
47. Nilges, M., Clore, G. M., and Gronenborn, A. M. (1988) *FEBS Lett. 229*, 317−324.
48. Brünnger, A. T. (1993) *XPLOR* Version 3.1 Manual, Yale University, New Haven, CT.
49. Garrett, D. S., Kuszewski, J., Hancock, T. J., Lodi, P. J., Vuister, G. W., Gronenborn, A. M., and Clore, G. M. (1994) *J. Magn. Reson. B 104*, 99−103.
50. Kuszewski, J., Qin, J., Gronenborn, A. M., and Clore, G. M. (1995) *J. Magn. Reson. B 106*, 92−96.
51. Hoog, J. O., Holmgren, A., D′Silva, C., Douglas, K. T., and Seddon, A. P. (1982) *FEBS Lett. 138*, 59−61.
52. Wishart, D. S., Sykes, B. D., and Richard, F. M. (1991) *J. Mol. Biol. 222*, 311−333.
53. Spera, S., and Bax, A. (1991) *J. Am. Chem. Soc. 113*, 5490−5492.
54. Sun, C., Holmgren, A., and Bushweller, J. H. (1997) *Protein Sci. 6*, 383−390.
55. Qin, J., Clore, G. M., Kennedy, W. M. P., Huth, R., and Gronenborn, A. M. (1995) *Structure 3*, 289−297.
56. Richardson, J. S. (1981) *Adv. Protein Chem. 34*, 167−330.
57. Hol, W. G. J. (1985) *Prog. Biophys. Mol. Biol. 45*, 149−195.
58. Kraulis, P. J. (1991) *J. Appl. Crystallogr. 24*, 946−950.

BI9806504